Ba$_3$$M_xTi_{3-x}O_9$ ($M =$ Ir, Rh): A family of 5d/4d-based diluted quantum spin liquids

R. Kumar,[1] D. Sheptyakov,[2] P. Khuntia,[3,4] K. Rolfs,[5] P. G. Freeman,[6,7] H. M. Rønnow,[6] Tusharkanti Dey,[1,8]
M. Baenitz,[4] and A. V. Mahajan[1,*]

[1]*Department of Physics, Indian Institute of Technology Bombay, Powai, Mumbai 400076, India*
[2]*Laboratory for Neutron Scattering and Imaging, Paul Scherrer Institut, 5232 Villigen-PSI, Switzerland*
[3]*Laboratoire de Physique des Solides Universite Paris-Sud, UMR CNRS91405 Orsay, France*
[4]*Max-Planck Institute for Chemical Physics of Solids, 01187 Dresden, Germany*
[5]*Laboratory for Developments and Methods, Paul Scherrer Institut, 5232 Villigen PSI, Switzerland*
[6]*Laboratory for Quantum Magnetism, Ecole Polytechnique Federale de Lausanne (EPFL), CH 1015, Switzerland*
[7]*Jeremiah Horrocks Institute for Mathematics, Physics and Astronomy, University of Central Lancashire, Preston, PR1 2HE United Kingdom*
[8]*Experimental Physics VI, Center for Electronic Correlations and Magnetism, University of Augsburg, D-86159 Augsburg, Germany*

We report the structural and magnetic properties of the 4d ($M =$ Rh) based and 5d ($M =$ Ir) based systems Ba$_3$$M_xTi_{3-x}O_9$ (nominally $x = 0.5$, 1). The studied compositions were found to crystallize in a hexagonal structure with the centrosymmetric space group $P6_3/mmc$. The structures comprise of A_2O$_9$ polyhedra [with the A site (possibly) statistically occupied by M and Ti] in which pairs of transition metal ions are stacked along the crystallographic c axis. These pairs form triangular bilayers in the ab plane. The magnetic Rh and Ir ions occupy these bilayers, diluted by Ti ions even for $x = 1$. These bilayers are separated by a triangular layer which is dominantly occupied by Ti ions. From magnetization measurements we infer strong antiferromagnetic couplings for all of the materials but the absence of any spin-freezing or spin-ordering down to 2 K. Further, specific heat measurements down to 0.35 K show no sign of a phase transition for any of the compounds. Based on these thermodynamic measurements we propose the emergence of a quantum spin liquid ground state for Ba$_3$Rh$_{0.5}$Ti$_{2.5}$O$_9$, and Ba$_3$Ir$_{0.5}$Ti$_{2.5}$O$_9$, in addition to the already reported Ba$_3$IrTi$_2$O$_9$.

I. INTRODUCTION

Transition metal oxides (TMOs) containing 4d and 5d metal atoms are of continuing interest and are being explored extensively [1]. In particular, 5d-based TMOs are believed to host various exotic ground states because of a relatively weak on-site Coloumb repulsion U (compared to typical values for 3d TMOs) and a strong spin-orbit coupling (SOC) λ. Also, it is now well recognized that an intricate competition among the three energy scales (a) on-site Coulomb repulsion (U), (b) crystal-field splitting (Δ), and (c) SOC, opens up avenues for the existence of a diverse spectrum of physical properties [1,2]. Among such exotic ground states, quantum spin liquids (QSL) are being widely discussed. The quantum spin liquid state is a highly entangled state of localized moments that does not break any symmetry of the Hamiltonian down to $T = 0$ K [3]. The experimental signatures of the QSL state have been suggested to be (i) a Curie-Weiss susceptibility [$C/(T - \theta)$] with a negative θ, (ii) no indication of spin ordering or spin freezing such as a peak in the temperature dependence of susceptibility or the presence of a bifurcation in the field cooled and zero-field cooled susceptibility below some temperature or perhaps a large "frustration ratio" $f = |\theta/T_N|$, where T_N is the ordering temperature, (iii) absence of a peak in the temperature dependence of heat capacity but the presence of a magnetic contribution to the heat capacity with a power law behavior in temperature, etc. While 3d-based TMOs include several materials with QSL [3] behavior, very few examples of 4d/5d-based QSLs have been reported. Prior

to the work of Dey *et al.* on Ba$_3$IrTi$_2$O$_9$ [4] and Ba$_3$YIr$_2$O$_9$ (HP phase) [5], to our knowledge, Na$_4$Ir$_3$O$_8$ [6] was the only reported QSL among 5d-based TMOs. However, it appears that, no such dynamically disordered ground state manifold has been realized so far in 4d-based TMOs, where U and SOC are expected to be of comparable strengths. Ba$_2$YMoO$_6$ [7–10] drew considerable attention, but it does not fulfill the criteria of a QSL and subsequent measurements suggest this to be a valence bond glass (VBG) rather than a QSL.

The Ba$_3$$MX_2O_9$ series with $M =$ Co, Ni, Cu, Ru, Ir and $X =$ Sb, Ti, [4,11–14] displays a variety of ground states depending upon the electronic states of the ions, strength of the SOC, and the crystal-field energy. However, Ba$_3$ZnIr$_2$O$_9$, where Ir is in the pentavalent oxidation state, shows a spin-orbital liquid state because of the comparable energy scales induced by the SOC and superexchange interactions [15]. Dey *et al.* [4] studied a $J_{\rm eff} = 1/2$ two-dimensional (2D) Mott insulator Ba$_3$IrTi$_2$O$_9$, which has significant Ir/Ti site disorder resulting in an effective dilution of the magnetic Ir^{4+} planes. Nevertheless, it appears to be an example of a spin-orbit driven spin liquid, which does not order down to 0.35 K inspite of a large antiferromagnetic Curie-Weiss temperature $\theta_{\rm CW}$ (~ -107 K). Very recently, Ba$_3$IrTi$_2$O$_9$ has also evinced theoretical interest and Becker *et al.* [16] proposed it to be a model example to realize the Heisenberg-Kitaev model on a triangular lattice. Catuneanu *et al.* [17] predicted Ba$_3$IrTi$_2$O$_9$ to host a stripy ordered magnetic ground state. Many of the materials in the Ba$_3$$MX_2O_9$ series including Ba$_3$CuSb$_2$O$_9$ [18], Ba$_3$IrTi$_2$O$_9$ [4], and Ba$_3$RuTi$_2$O$_9$ [14] exhibit atomic site disorder. According to a recent theoretical proposal of Smerald *et al.* [19] correlated lattice disorder along with delocalized orphan spins can promote a spin-orbital

*mahajan@phy.iitb.ac.in

liquid phase, and this was suggested to be the case for $Ba_3CuSb_2O_9$ [13,18,20]. The recent theoretical interest to underline the basic physics behind the family of materials with formula $Ba_3MX_2O_9$ (M = Co, Ni, Cu, Ru, Ir and X = Sb, Ti), further motivates us to explore these materials in detail.

Our present study focusses on $Ba_3M_xTi_{3-x}O_9$ (nominally $x = 0.5, 1$), where M = Ir, Rh. The $Ba_3IrTi_2O_9$ system was previously reported to crystallize in the hexagonal space group $P6_3mc$ (186). In this space group, Ir^{4+} ($5d^5$, $J_{eff} = 1/2$) and Ti^{4+} ($S = 0$) occupy the $2b$ sites and form structural dimers (along the c direction) which then form triangular biplanes (ab plane) with an ordered arrangement of Ir and Ti. Between successive biplanes there is a nonmagnetic triangular layer of Ti-atoms at the $2a$ sites [4]. Due to their similar ionic radii, however, it is inevitable to have mixing among Ir^{4+} and Ti^{4+} site occupancies and Rietveld refinement carried out on x-ray data suggested this intersite disorder.

Here, we present neutron diffraction measurements carried out on $Ba_3IrTi_2O_9$ and refinement with a higher-symmetry space group $P6_3/mmc$ (the metal ions in the dimers are disordered in this case), which reveals that approximately 56% of the $4f$ (1/3, 2/3, z) Wyckoff positions are occupied by nonmagnetic Ti atoms, while the remaining 44% are occupied by magnetic Ir atoms. This gives rise to depleted biplanes. An idealized depiction (equal but disordered occupation of $4f$ sites by M and Ti and sole occupation of $2a$ sites by Ti) of $Ba_3MTi_2O_9$ (M = Ir, Rh) in the space group $P6_3/mmc$ can be seen in Fig. 1.

While $Ba_3IrTi_2O_9$, $Ba_3Ir_{0.5}Ti_{2.5}O_9$, and $Ba_3Rh_{0.5}Ti_{2.5}O_9$ could be prepared in single phase form, $Ba_3RhTi_2O_9$ contained large amounts of impurities. The large dilution which is naturally present even for the nominal $x = 1$ composition brings the system in proximity of the percolation threshold (site percolation: $p_c = 0.5$) (see Ref. [21]) of a 2D triangular lattice. For
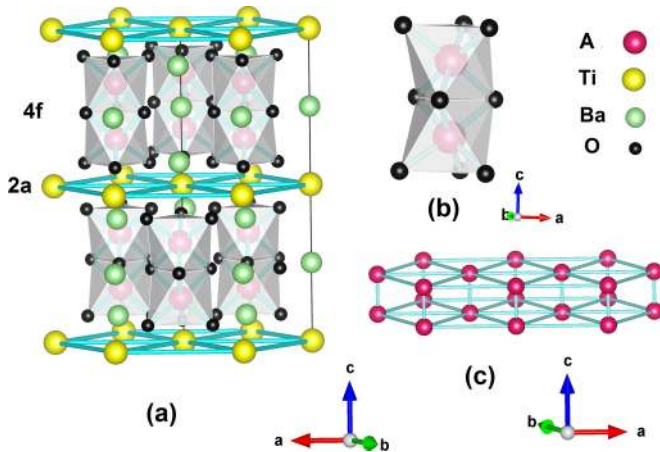
the presented materials, having triangular bilayers, the percolation threshold might be somewhat smaller. In any case, in the systems studied by us (single-phase samples of nominal composition $Ba_3IrTi_2O_9$, $Ba_3Ir_{0.5}Ti_{2.5}O_9$, and $Ba_3Rh_{0.5}Ti_{2.5}O_9$), no ordering or freezing occurs down to 0.35 K. The novelty of these compounds is that even with such a large dilution (only about 25% magnetic atoms in the bilayers for the latter two), their magnetic susceptibilities show a Curie-Weiss behavior with a large Curie-Weiss temperature (similar θ_{CW} for all the three systems), and no ordering or freezing down to 0.35 K. From our heat capacity measurements, we find that there is a magnetic contribution to the heat capacity with a power-law variation with temperature. Our present investigation suggests that the systems maintain a QSL state down to 0.35 K.

II. EXPERIMENTAL DETAILS

Polycrystalline samples of nominal stoichiometry $Ba_3IrTi_2O_9$, $Ba_3Ir_{0.5}Ti_{2.5}O_9$, $Ba_3RhTi_2O_9$, and $Ba_3Rh_{0.5}Ti_{2.5}O_9$ were prepared by conventional solid state reaction methods using high purity starting materials: $BaCO_3$ (Alfa Aessar, 99.95%), TiO_2 (Alfa Aessar, 99.9%), Ir (Arro Biochem, 99.9%), and Rh (Alfa Aessar, 99.95%) metal powder. As will be detailed in the next section, for nominal compositions of $Ba_3IrTi_2O_9$, $Ba_3Ir_{0.5}Ti_{2.5}O_9$, $Ba_3RhTi_2O_9$, and $Ba_3Rh_{0.5}Ti_{2.5}O_9$, the refined compositions were found to be $Ba_3Ir_{0.946}Ti_{2.054}O_9$, $Ba_3Ir_{0.484}Ti_{2.516}O_9$, $Ba_3Rh_{0.593}Ti_{2.407}O_9$, and $Ba_3Rh_{0.432}Ti_{2.568}O_9$, respectively.

Powder x-ray diffraction (xrd) measurements were performed at room temperature with Cu K_α radiation (λ = 1.54182 Å) on a PANalytical X' Pert PRO diffractometer. Neutron diffraction (ND) measurements were performed on the HRPT diffractometer [22] at the SINQ neutron source of the Paul Scherrer Institut (PSI) on the aforementioned polycrystalline samples at 300 and 1.5 K. In order to reduce the neutron absorption, the samples ($Ba_3IrTi_2O_9$ and $Ba_3RhTi_2O_9$) were mounted in a vanadium sample can of 5.5 mm diameter, while $Ba_3Ir_{0.5}Ti_{2.5}O_9$ and $Ba_3Rh_{0.5}Ti_{2.5}O_9$ were mounted in a vanadium can of 7.5 mm diameter with a sample height of approximately 30 mm. Incident neutron wavelengths of 1.15, 1.494, and 1.88 Å were selected from a Bragg reflection from a Ge monochromator, with a pyrolytic graphite filter placed in the incident beam to remove higher-order neutrons. The samples were mounted in a standard orange cryostat. The scattered neutrons were detected over an angular range $(2\theta)3.75°–164.7°$ by a ^{3}He multidetector. A radial collimator was placed between the sample and detectors to stop neutrons scattered from the sample environment from reaching the detectors.

Magnetization measurements were carried out in the temperature range 2–400 K and the field range 0–70 kOe using a Quantum Design SVSM. Heat capacity measurements were performed in the temperature range 0.35–295 K and in the field range 0–90 kOe using the heat capacity option of a Quantum Design PPMS.

FIG. 1. Schematic representation of the crystal structure of $Ba_3MTi_2O_9$ (M=Ir, Rh) in the space group $P6_3/mmc$. (a) An ideal unit cell, i.e., with the $4f$ site equally occupied by Ir (or Rh) and Ti and the $2a$ site occupied by Ti only. (b) The structure of a A_2O_9 polyhedron (where A corresponds to M and Ti with a 50% probability each), consisting of two face sharing AO_6 octahedra, thus forming the M-Ti, M-M, or Ti-Ti dimers. (c) Formation of bitriangular planes containing an equal amount the nonmagnetic Ti and magnetic (Ir or Rh) atoms in the $4f$ (1/3,2/3,z) positions.

III. RESULTS

In this section, we present the results of our systematic structural, magnetic, and heat capacity measurements on the

samples with nominal compositions mentioned in the previous section.

A. Ba$_3$IrTi$_2$O$_9$ and Ba$_3$Ir$_{0.5}$Ti$_{2.5}$O$_9$

1. Crystal structures

The crystal structures of Ba$_3$IrTi$_2$O$_9$ and Ba$_3$Ir$_{0.5}$Ti$_{2.5}$O$_9$ have been investigated, with particular emphasis on the precise quantification of the metal site occupation by Ir and Ti atoms. Both compounds display impurity-free patterns and their refinements were carried out with the FULLPROF SUITE [23]. The typical refinement plots for both the parent (Ba$_3$IrTi$_2$O$_9$) and its magnetically diluted version (Ba$_3$Ir$_{0.5}$Ti$_{2.5}$O$_9$) are presented in Figs. 2(a) and 2(b), respectively. A strong contrast in scattering lengths between Ir and Ti (10.6 and -3.438 fm) [24] allows for a sufficiently high precision in determining the partial occupations of Ir and Ti atoms at the $2a$ and $4f$ sites, respectively, for the nominal $x = 1$ composition. However, for the nominal $x = 0.5$ composition, the small Ir : Ti ratio leads to a rather low average scattering length, thus making the refinement of positional and atomic displacement parameters less reliable or impossible. The crystal structure of Ba$_3$IrTi$_2$O$_9$ was reported by Dey *et al.* (see Ref. [4]) to have the space group $P6_3mc$ (No. 186, noncentrosymmetric). We have carried out extensive refinements in both $P6_3mc$ and $P6_3/mmc$ (No. 194a, centrosymmetric, higher-symmetry supergroup of $P6_3mc$) and we find that actually both choices lead to equally good refinements, and essentially identical structures. The crystallographic sites occupied by the Ti : Ir atoms in $P6_3/mmc$ space group model are $2a$ (0,0,0) and

$4f$ (1/3,2/3,z). In the noncentrosymmetric subgroup $P6_3mc$, they transform into the $2a$ (0,0,z) (a site with floating z coordinate), and into a pair of $2b$ (1/3,2/3,z) sites correspondingly. Of significant importance would be any statistically meaningful deviations in the refined geometries and/or in the partial Ir : Ti occupations on the metal sites, especially for the two individual metal positions in the A_2O$_9$ double octahedral layers. However, from our refinements in the lower-symmetry $P6_3mc$ space group it follows that for both Ba$_3$IrTi$_2$O$_9$ and Ba$_3$Ir$_{0.5}$Ti$_{2.5}$O$_9$, we get essentially identical crystal structures as in the higher symmetry $P6_3/mmc$.

This in particular implies that the partial Ir : Ti occupations of both metal positions in the dimer layer of the face-sharing MO$_6$ octahedra refine to the same values. Also, the refinement agreement factors for the structure models for both space groups are practically indistinguishable, which is why we consider it to be justified to refine the crystal structure parameters of Ba$_3$IrTi$_2$O$_9$ and Ba$_3$Ir$_{0.5}$Ti$_{2.5}$O$_9$ in a model assuming the higher-symmetry space group $P6_3/mmc$ (No. 194). The refined unit cell parameters at 300 K ({a,c} = {5.7197(2) Å, 14.0564(5) Å} and {5.7239(2) Å, 14.0074(5) Å} for Ba$_3$IrTi$_2$O$_9$ and Ba$_3$Ir$_{0.5}$Ti$_{2.5}$O$_9$, correspondingly) are in good agreement with the previously reported results [4]. The refined crystal structure parameters are listed in Table I. The main finding is that in both compounds, the metal sites $2a$ (0,0,0) are predominantly occupied by Ti atoms (refined occupation ratios of Ir to Ti are 0.064(4) : 0.936(4) for Ba$_3$IrTi$_2$O$_9$ and 0.000(5) : 1.000(5) for Ba$_3$Ir$_{0.5}$Ti$_{2.5}$O$_9$). In the double layers of the stacked face-sharing AO$_6$ octahedra, the n (Ir : Ti) ratios are 0.441(2) : 0.559(2) and 0.242(3) : 0.758(3) for Ba$_3$IrTi$_2$O$_9$ and Ba$_3$Ir$_{0.5}$Ti$_{2.5}$O$_9$, correspondingly, thus providing the final refined stoichiometries of the two compounds: Ba$_3$Ir$_{0.946}$Ti$_{2.054}$O$_9$ and Ba$_3$Ir$_{0.484}$Ti$_{2.516}$O$_9$. These results imply that Ir concentration in the biplanes in the Ba$_3$Ir$_{0.5}$Ti$_{2.5}$O$_9$ compound is 24 %, while in the Ba$_3$IrTi$_2$O$_9$ compound, the biplanes have 44 % iridium. The $2a$ (0,0,0) Wyckoff position is occupied by 6% Ir atoms.

The obtained atomic coordinates and occupancies refined for Ba$_3$IrTi$_2$O$_9$ with $P6_3/mmc$ space group are listed in Table I. The main difference between the structure of Ba$_3$$MTi_2O_9$, as per the space groups $P6_3/mmc$ or $P6_3mc$ arises as a result of the arrangement of magnetic atoms in $4f$ and $2b$ Wyckoff positions, respectively. The $4f$ Wyckoff position in $P6_3/mmc$ has a disordered occupation by M and Ti atoms giving rise to A_2O$_9$ polyhedra composed of two face sharing AO$_6$ [see Fig. 1(b)], where A corresponds to M and Ti with a 50% probability each. The A_2O$_9$ polyhedra make up triangular biplanes [see Fig. 1(c)], which are 50% diluted. In contrast, the $2b$ Wyckoff positions in $P6_3mc$ have Ir making undiluted single triangular planes (ab plane) in the ideal case.
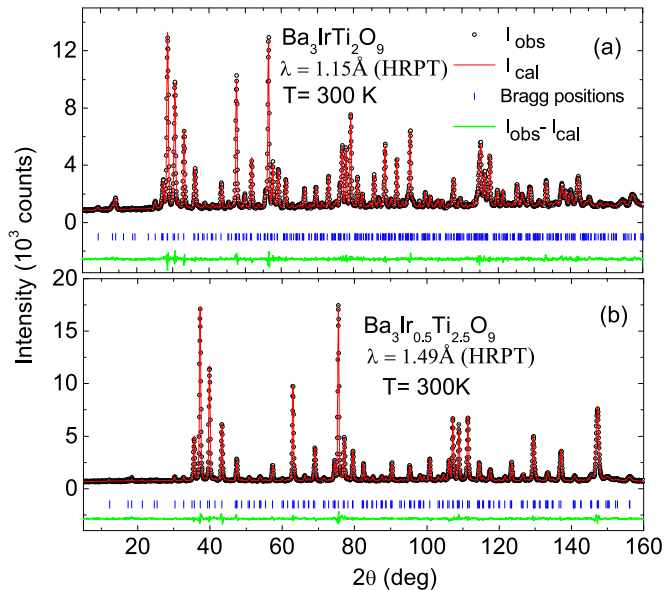
2. Magnetic susceptibility

Magnetic susceptibility (as also its inverse) for nominal Ba$_3$Ir$_{0.5}$Ti$_{2.5}$O$_9$ is shown in Fig. 3. For clarity, only the inverse susceptibility variation with temperature is shown for nominal Ba$_3$IrTi$_2$O$_9$. As illustrated in the inset of Fig. 3, the magnetization measurements on Ba$_3$Ir$_{0.5}$Ti$_{2.5}$O$_9$ in a 25 Oe field do not evidence any bifurcation of the zero field cooled (ZFC) and field cooled (FC) data. In contrast, a

FIG. 2. Typical Rietveld refinement plots. (a) The neutron diffraction data collected for Ba$_3$IrTi$_2$O$_9$ at 300 K with wavelength $\lambda = 1.15$ Å and (b) with wavelength $\lambda = 1.49$ Å for Ba$_3$Ir$_{0.5}$Ti$_{2.5}$O$_9$. Experimental points (black open circles), calculated patterns (red lines) and difference curves (green lines) are shown, the ticks (blue vertical lines) below the graphs indicate the calculated positions of Bragg peaks. It should be noted that the green lines on y axis are shifted for clarity.

TABLE I. Refined crystal structure parameters of $Ba_3IrTi_2O_9$ and $Ba_3Ir_{0.5}Ti_{2.5}O_9$. Space group $P6_3/mmc$ (No. 194), atoms are in the following Wyckoff positions: Ba1 in $2b$ $(0,0,1/4)$, Ba2 and (Ir/Ti)1 in $4f$ $(1/3,2/3,z)$, (Ir/Ti)2 in $2a$ $(0,0,0)$, O1 in $6h$ $(x,2x,1/4)$, and O2 in $12k$ $(x,2x,z)$. Results obtained from neutron powder data collected at 300 K with wavelengths $\lambda = 1.1545$ Å ($Ba_3IrTi_2O_9$) and $\lambda = 1.494$ Å ($Ba_3Ir_{0.5}Ti_{2.5}O_9$). Refined exact stoichiometries of the two compounds are $Ba_3Ir_{0.946}Ti_{2.054}O_9$ and $Ba_3Ir_{0.484}Ti_{2.516}O_9$.

Atoms		$Ba_3IrTi_2O_9$	$Ba_3Ir_{0.5}Ti_{2.5}O_9$
	a, Å	5.7197(2)	5.7239(1)
	c, Å	14.0564(5)	14.0070(2)
	V, Å^3	398.25(3)	397.43(1)
Ba1	B_{iso}, Å^2	0.73(7)	0.54(5)
Ba2	z	0.5956(2)	0.5971(2)
	B_{iso}, Å^2	0.73(4)	0.69(3)
(Ir/Ti)1	z	0.1606(3)	0.1606 [a]
	n (Ir:Ti)	0.441(2):0.559(2)	0.242(3):0.758(3)
	B_{iso}, Å^2	0.21(6)	1.6 [b]
(Ir/Ti)2	n (Ir:Ti)	0.064(4):0.936(4)	0.000(5):1.000(5)
	B_{iso}, Å^2	0.88(12)	1.6(1)
O1	x	0.4854(5)	0.4842(3)
	B_{iso}, Å^2	0.76(3)	0.90(2)
O2	x	0.1648(4)	0.1655(3)
	z	0.0795(1)	0.0799(1)
	B_{iso}, Å^2	0.86(2)	0.94(2)
	R_p	2.91%	3.63%
	R_{wp}	3.68%	4.75%
	R_{exp}	2.44%	2.81%
	χ^2	2.27	2.86
overall refined	n (Ir:Ti)	0.946(6):2.054(6)	0.484(8):2.516(8)

[a]The z coordinate for this position could not be refined because of the unfavorable average scattering length for this combination of Ti:Ir occupations (see text). It has therefore been fixed to the value refined for $Ba_3IrTi_2O_9$.

[b]for the same reason, this parameter was not refined, but instead fixed to the value refined for the (Ti/Ir)2 position.

clear opening was observed at 80 K for the parent compound $Ba_3IrTi_2O_9$ which, however closed (see supplemental information of Ref. [4]) on increasing the field to 500 Oe [4]. The susceptibility fit for $Ba_3Ir_{0.5}Ti_{2.5}O_9$ with the Curie-Weiss law, $\chi = \chi_0 + C/(T - \theta_{CW})$, in the temperature range 150–400 K yields a negative value of the asymptotic Curie-Weiss temperature $\theta_{CW} \sim -125$ K and a temperature independent susceptibility $\chi_0 = -2.873 \times 10^{-5}$ cm^3/mole Ir. Furthermore, a reduced value of the effective magnetic moment $\mu_{eff} = 1.32 \pm 0.05 \mu_B$ was determined compared to the expected $1.73 \mu_B$ for a $S = 1/2$ moment. In fact, the parent, undiluted compound shows an even bigger quenching of the magnetic moment ($\mu_{eff} = 1.05 \pm 0.04 \mu_B$ and $\theta_{CW} \sim -107$ K). A reduced μ_{eff} appears to be common among iridates and might be a consequence of SOC. It is not clear as to why a 50% magnetic dilution helps in increasing the moment value.
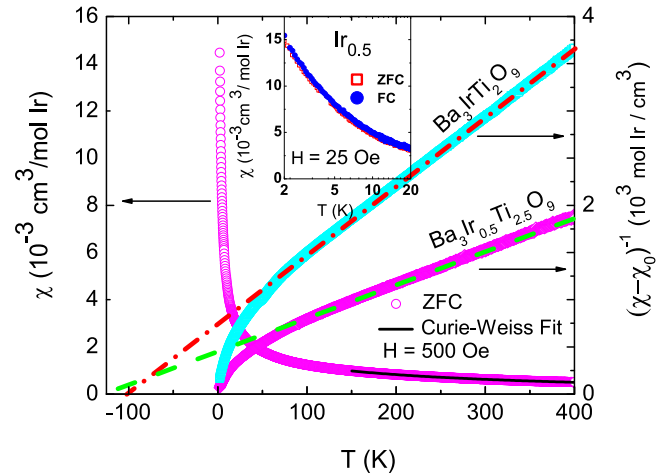

FIG. 3. The left y-axis shows the temperature dependent susceptibility of nominal $Ba_3Ir_{0.5}Ti_{2.5}O_9$ measured in 500 Oe in the temperature range 2–400 K and the black solid line represents the Curie-Weiss fit in the temperature range 150–400 K. The right y-axis depicts the T dependence of inverse dc susceptibility of the parent compound $Ba_3IrTi_2O_9$(nominal) and its diluted variant $Ba_3Ir_{0.5}Ti_{2.5}O_9$. Inset shows the ZFC and FC data recorded in the temperature range 2–20 K at 25 Oe for $Ba_3Ir_{0.5}Ti_{2.5}O_9$ in a linear-log plot.

3. Heat capacity

To explore further the ground-state properties of nominal $Ba_3Ir_{0.5}Ti_{2.5}O_9$, we examined heat capacity $C_P(T)$ data in various fields (0–140 kOe), as shown in Fig. 4(a). No anomaly, hallmark of any short-range or long-range magnetic ordering, was observed in the $C_P(T)$ data in the measured temperature range. However, below about 10 K, $C_P(T)$ data show a broad maximum, which shifts towards higher-T upon increasing the magnetic field indicating that it might be a Schottky contribution originating from orphan spins as is apparently
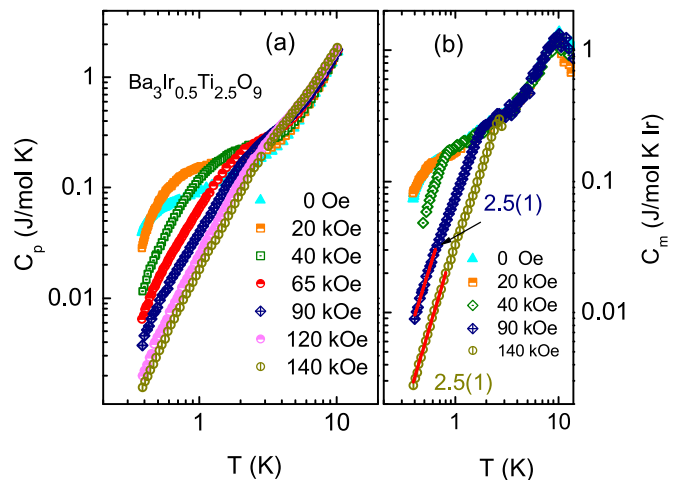

FIG. 4. (a) The $C_p(T)$ data for $Ba_3Ir_{0.5}Ti_{2.5}O_9$ (baked) is depicted in the log-log plot as a function of temperature at different fields. (b) The magnetic heat capacity C_m is shown in a log-log plot and the solid lines are fits to the power law: $C_m = \gamma T^\alpha$ (explained in the text). The obtained exponent values are written against the C_m data.
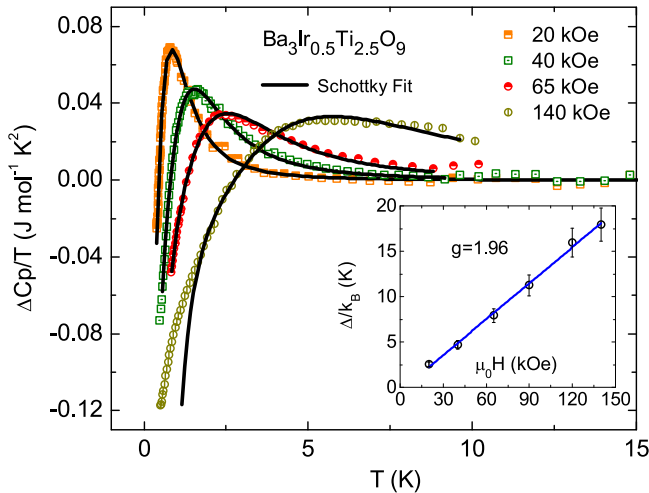
FIG. 5. A few representative plots of $[C_P(H) - C_P(H = 0)]/T$ or $(\triangle C_P/T)$ for Ba$_3$Ir$_{0.5}$Ti$_{2.5}$O$_9$ at various values of the field H (as given in the legend) and their fit to Eq. (1) (black lines). (Inset) Variation of the Schottky gap as a function of magnetic field for orphan spins.

very common for disordered materials. These orphan spins can arise from (a) Ir occupying the 2a sites and (b) a small fraction of uncompensated Ir^{4+} spins from the triangular bilayers. Such orphan spins then might form a two-level system and in turn show a field dependence at low T. This behavior was also noticed in the parent compound Ba$_3$IrTi$_2$O$_9$ (nominal) [4].

The specific heat of a magnetic insulator in the presence of orphan spins comprises of (a) specific heat due to the lattice (C_{lattice}), (b) specific heat due to uncorrelated spins or the Schottky specific heat (C_{Sch}), and (c) specific heat due to correlated magnetic spins (C_m). In the absence of a suitable nonmagnetic analog, C_{lattice} for Ba$_3$Ir$_{0.5}$Ti$_{2.5}$O$_9$ was estimated by adopting Ba$_3$ZnSb$_2$O$_9$ as the nonmagnetic analog. The $C_P(T)$ data for Ba$_3$ZnSb$_2$O$_9$ were extracted from Ref. [13]. The heat capacity of this nonmagnetic analog was scaled to match with the heat capacity of Ba$_3$Ir$_{0.5}$Ti$_{2.5}$O$_9$ in the temperature range 20–45 K. The corrected heat capacity of Ba$_3$ZnSb$_2$O$_9$ thus obtained was subtracted from the measured heat capacity of Ba$_3$Ir$_{0.5}$Ti$_{2.5}$O$_9$. This yielded $C_{\text{Sch}} + C_m$.

To remove the Schottky contribution from $C_P(T)$ data, the following strategy was adopted: first we subtracted the $C_P(H = 0)$ data from those measured in $H \neq 0$, i.e., $C_P(H)$. This difference ($\triangle C_P/T$) was modeled as a function of temperature using $[C_{\text{Sch}}(\triangle_1) - C_{\text{Sch}}(\triangle_2)]f/T$, where f stands for the percentage of orphan spins present in the sample and $C_{\text{Sch}}(\triangle_1)$ and $C_{\text{Sch}}(\triangle_2)$ are the Schottky contributions to the specific heat. Figure 5 shows the estimated contribution as well as its variation [using Eq. (1)] as a function of temperature for several magnetic fields. The parameters $\triangle_1$ and $\triangle_2$ are the values of energy separation under the influence of external magnetic fields H_1 and $H_2(=0$ Oe$)$, respectively. Furthermore, C_{Sch} is defined by the equation

$$C_{\text{Sch}}(\triangle) = R\left(\frac{\triangle}{k_BT}\right)^2\left(\frac{g_0}{g_1}\right)\frac{\exp\left(\frac{\triangle}{k_BT}\right)}{\left[1 + \left(\frac{g_0}{g_1}\right)\exp\left(\frac{\triangle}{k_BT}\right)\right]^2} \quad (1)$$

Here, R and k_B are the universal gas constant and the Boltzmann constant, respectively. The parameters g_0 and g_1 are the degeneracies of the two level system and in the present case are assumed to be unity. This routine process to eliminate the orphan spin contribution has already been used earlier in materials such as Ba$_3$CuSb$_2$O$_9$ [13] and ZnCu$_3$(OH)$_6$Cl$_2$ [25]. While estimating the Schottky contribution, the parameters $\triangle_1$, $\triangle_2$ and f were kept free and the variation of $\triangle_1$ for various magnetic fields is shown in the inset of Fig. 5. The parameter $\triangle_2$ was found to vary between 0.3 and 1.44 K (not significantly different from zero) in the field range 20–140 kOe. The extracted value of f for Ba$_3$Ir$_{0.5}$Ti$_{2.5}$O$_9$ amounts to 3%–4% and might come from Ir^{4+} spins. Estimated g value (see inset of Fig. 5) obtained for orphan spins is 1.96, which is the free spin only value suggesting that orphan spins might not be affected by SOC.

Finally, the inferred C_m is plotted in Fig. 4(b). In an attempt to shed some light on the nature of magnetic excitations at low T, the C_m data were fitted with the equation $C_m = \gamma T^\alpha$. The obtained value of α for $T \leqslant 1$ K varies somewhat with H but is nearly constant at about 2.5 in high fields. Such H-dependent behavior of C_m was also observed for compound Ba$_3$IrTi$_2$O$_9$ [4]. An uncertainty in determining C_{Sch} at lower fields, where the Schottky hump lies at low T might affect the value of α. However, for $H \geqslant 90$ kOe, where the Schottky hump shifts to higher T, the obtained α for $T \leqslant 1$K remains unaffected by C_{Sch} because of its vanishingly small contribution to $C_P(T)$.

The magnetic entropy change $\triangle S_m$ was calculated by integrating $\frac{C_m}{T}$ versus T data for the Ba$_3$Ir$_{0.5}$Ti$_{2.5}$O$_9$ sample, as shown in Fig. 10. The calculated $\triangle S_m$ in zero field was found to be 1.76 (J/K mol Ir) below 25 K, which is nearly 30% of $R\ln 2 = 5.76$ J/mol K, expected for a $S = 1/2$ system. In contrast, for Ba$_3$IrTi$_2$O$_9$, it is 10% of what is expected for a $S = 1/2$ system. This suggests that the diluted compound is less magnetically disordered but the higher effective moment in the Ba$_3$Ir$_{0.5}$Ti$_{2.5}$O$_9$ system may also play a role.

B. Ba$_3$RhTi$_2$O$_9$ and Ba$_3$Rh$_{0.5}$Ti$_{2.5}$O$_9$

1. Crystal structure

In the following section, we focus on the 4d-based Ba$_3$Rh$_x$Ti$_{3-x}$O$_9$, which is isostructural to the 5d-based Ba$_3$IrTi$_2$O$_9$. The Ba$_3$RhTi$_2$O$_9$ was first reported by Byrne *et al.* [26] and its xrd pattern was claimed to be similar to that of the hexagonal BaTiO$_3$ but also containing some secondary, unidentified phase(s). However, no further detailed information on the crystal structure of Ba$_3$RhTi$_2$O$_9$ was provided. Our laboratory x-ray diffraction pattern (not shown) of the nominal Ba$_3$RhTi$_2$O$_9$ has shown the extra lines as well, which were identified as coming from Ba$_9$Rh$_8$O$_{24}$ impurity [27]. Even with this impurity introduced into the refinement, there are still a few spurious lines in the pattern, due to low amounts of other impurities. Neutron powder diffraction is again of great advantage for studying the crystal structure of Ba$_3$Rh$_x$Ti$_{3-x}$O$_9$, since the difference in neutron scattering lengths between Rh and Ti (5.88 and -3.438 fm) [24] allows for precise quantification of the partial occupations of Rh and Ti in different metal sites. Neutron powder diffraction data for the compound with the intended composition Ba$_3$RhTi$_2$O$_9$
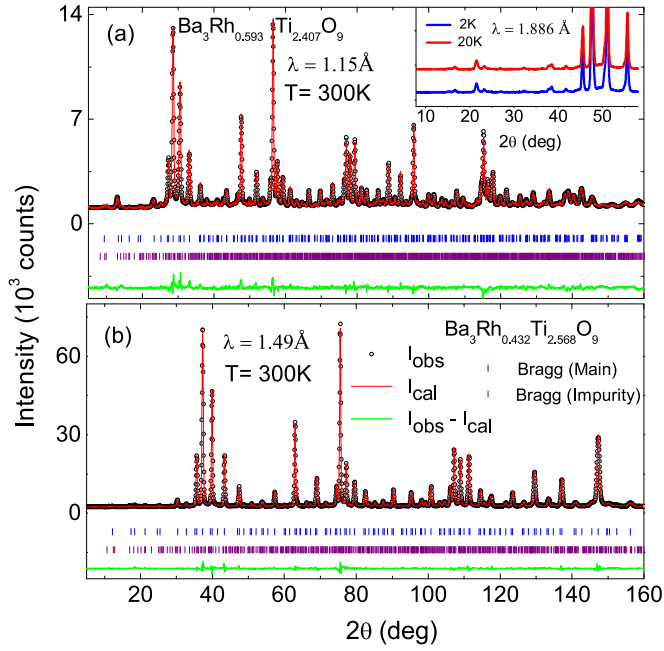
FIG. 6. The neutron diffraction data collected at 300 K for (a) nominal $Ba_3RhTi_2O_9$ (in actuality $Ba_3Rh_{0.593}Ti_{2.407}O_9$) with $\lambda = 1.15$ Å and (b) nominal $Ba_3Rh_{0.5}Ti_{2.5}O_9$ (in actuality $Ba_3Rh_{0.432}Ti_{2.568}O_9$) with $\lambda = 1.49$ Å, are shown with open black circles and the red solid lines represent the Rietveld refined patterns. The Bragg positions for main and impurity phases ($Ba_9Rh_8O_{24}$) are shown by vertical blue and purple lines and the difference patterns are depicted with green lines, respectively. It should be noted that $Ba_3RhTi_2O_9$ (nominal) contains roughly 12% of impurity phase $Ba_9Rh_8O_{24}$, whereas its diluted variant $Ba_3Rh_{0.5}Ti_{2.5}O_9$ (nominal) possesses less than 1.5% of impurity phase of $Ba_9Rh_8O_{24}$. The inset shows a comparison of the low-angle ranges of the experimental neutron diffraction patterns of $Ba_3RhTi_2O_9$ at 20 and at 2 K with $\lambda = 1.886$ Å, indicating that no additional (magnetic) intensity can be observed at the lowest achieved temperature.

have been collected at 2 K with the wavelengths $\lambda = 1.155$ and 1.886 Å, at 20 K with $\lambda = 1.886$ Å, and at 300 K with $\lambda = 1.1545$ Å. The shorter wavelength data were collected mainly to achieve the best precision in the crystal structure refinements, while the purpose to collect longer wavelength data at 2 and 20 K was to make sure that no magnetic ordering would manifest itself in appearance of any additional diffraction intensity at the base temperature. Coherent with the observation of the laboratory x-ray measurement, we see the $Ba_9Rh_8O_{24}$ impurity ($\sim$12 wt.%), and a few weak additional spurious lines at essentially the same d-spacing values as in the laboratory x-ray data. Sample preparation under various conditions failed to produce a single phase sample of $Ba_3RhTi_2O_9$. Consequently, we do not report the magnetic and heat capacity data for $Ba_3RhTi_2O_9$. We note, just for completeness, that the refined composition of this compound is $Ba_3Rh_{0.593(13)}Ti_{2.407(18)}O_9$ (the deficit of rhodium is due to the large amount of Rh-rich $Ba_9Rh_8O_{24}$ impurity), and that we do not observe an appearance of any additional Bragg intensities at low Q values when cooling down from 20 to 2 K and thus—down to the precision of our experiment, we can also exclude an emergence of LRO in $Ba_3Rh_{0.593}Ti_{2.407}O_9$.

TABLE II. Refined crystal structure parameters of the two studied $Ba_3Rh_xTi_{3-x}O_9$ compounds at room temperature. Space group $P6_3/mmc$ (No. 194), atoms are in the following Wyckoff positions: Ba1 in $2b$ $(0,0,1/4)$, Ba2 and (Ti/Rh)1 in $4f$ $(1/3,2/3,z)$, (Ti/Rh)2 in $2a$ $(0,0,0)$, O1 in $6h$ $(x,2x,1/4)$, and O2 in $12k$ $(x,2x,z)$. Results obtained from neutron powder data collected at 300 K with wavelengths $\lambda = 1.1545$ Å (sample with target composition $Ba_3RhTi_2O_9$, left column) and $\lambda = 1.494$ Å (sample with target composition $Ba_3Rh_{0.5}Ti_{2.5}O_9$, right column). Refined exact stoichiometries of the two compounds are $Ba_3Rh_{0.593}Ti_{2.407}O_9$ and $Ba_3Rh_{0.432}Ti_{2.568}O_9$.

Target composition		$Ba_3RhTi_2O_9$	$Ba_3Rh_{0.5}Ti_{2.5}O_9$
refined (Rh:Ti) composition		0.593(13):2.407(13)	0.432(18):2.568(18)
$Ba_9Rh_8O_{24}$ impurity (wt. %)		12(1)	1.5(0.5)
	a, Å	5.7186(7)	5.7209(1)
	c, Å	14.0271(18)	14.0159(2)
	V, Å^3	397.26(9)	397.27(1)
Ba1	B_{iso}, Å^2	0.56(11)[a]	0.49(2)[a]
Ba2	z	0.5947(8)	0.5952(2)
	B_{iso}, Å^2	0.56(11)[a]	0.49(2)[a]
(Rh/Ti)1	z	0.143(6)	0.1480(5)
	n (Rh:Ti)	0.292(5):0.708(5)	0.212(7):0.788(7)
	B_{iso}, Å^2	1.0(2)[b]	0.57(6)
(Rh/Ti)2	n (Rh:Ti)	0.009(8):0.991(8)	0.008(5):0.992(5)
	B_{iso}, Å^2	1.0(2)[b]	0.57(6)[b]
O1	x	0.4840(17)	0.4839(3)
	B_{iso}, Å^2	0.69(9)	0.74(2)
O2	x	0.1653(14)	0.1648(2)
	z	0.0796(3)	0.0802(1)
	B_{iso}, Å^2	0.62(5)	0.67(1)
	R_p (%)	3.21	2.95
	R_{wp} (%)	4.02	3.98
	R_{exp} (%)	2.41	1.46
	χ^2	2.78	7.40

[a]The B_{iso} parameters for both Ba atoms were refined with constraint to equality.

[b]The B_{iso} parameters for both Ti:Ir atoms were refined with constraint to equality.

An example of a Rietveld refinement done on the powder neutron diffraction data of this compound collected at the base temperature is given in the Fig. 6(a). The refined crystal structure parameters at room temperature are given in Table II.

The second compound, with a target nominal composition $Ba_3Rh_{0.5}Ti_{2.5}O_9$, did show a much smaller amount ($<$1.5%) of $Ba_9Rh_8O_{24}$ impurity [27], and the refined composition is $Ba_3Rh_{0.432(18)}Ti_{2.568(18)}O_9$. The Rietveld refined pattern is shown in Fig. 6(b). Practically all crystal structure parameters (given in the right column in Table II) are very close to those found for $Ba_3Rh_{0.593}Ti_{2.407}O_9$. Thus, in our synthetic approaches, the $\sim$0.5 : 2.5 ratio between Rh and Ti amounts in the $Ba_3Rh_{1-x}Ti_{2+x}O_9$ structure seems to be a characteristic feature, the remaining Rh being dumped into the Rh-rich impurity (in our case $Ba_9Rh_8O_{24}$).

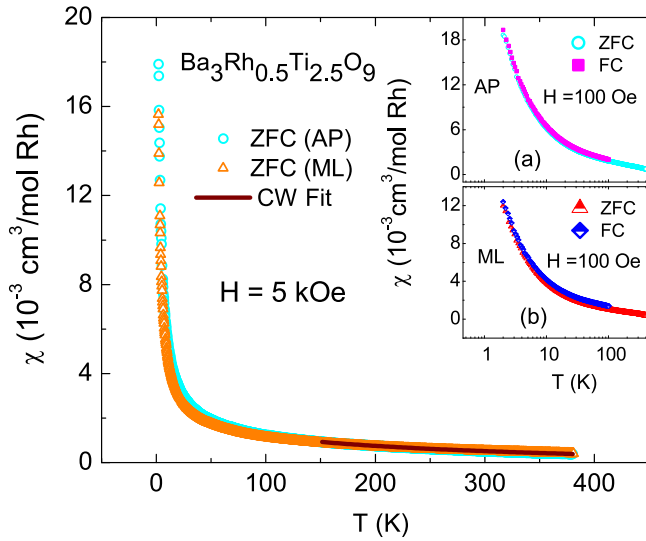FIG. 7. The main figure shows the temperature dependent susceptibilities of nominal Ba$_3$Rh$_{0.5}$Ti$_{2.5}$O$_9$ (AP) (cyan, open circles) and a month older batch of nominal Ba$_3$Rh$_{0.5}$Ti$_{2.5}$O$_9$ (ML) (orange, open triangles) measured in 5 kOe in the temperature range 2–400 K and the brown solid line represents the Curie-Weiss fit in the temperature range 150–400 K. Inset (a) and (b) depict the ZFC and FC data of nominal Ba$_3$Rh$_{0.5}$Ti$_{2.5}$O$_9$ (AP) and nominal Ba$_3$Rh$_{0.5}$Ti$_{2.5}$O$_9$ (ML) measured at 100 Oe, respectively.

From our results it follows that in both studied Ba$_3$Rh$_x$Ti$_{3-x}$O$_9$ compositions, the metal $2a(0,0,0)$ sites are practically exclusively occupied by titanium, while the Rh : Ti occupation factors ratio of roughly 1 : 3 is characteristic for the $4f(1/3,2/3,z)$ sites. This delivers the refined compositions Ba$_3$Rh$_{0.593}$Ti$_{2.407}$O$_9$ and Ba$_3$Rh$_{0.432}$Ti$_{2.568}$O$_9$ for the two studied compounds, thus indicating a stability (under our synthetic conditions) of the approximate Ba$_3$Rh$_{0.5}$Ti$_{2.5}$O$_9$ composition. Since the nominal Ba$_3$RhTi$_2$O$_9$ is not single phase, we report further measurements on only Ba$_3$Rh$_{0.5}$Ti$_{2.5}$O$_9$, which is single
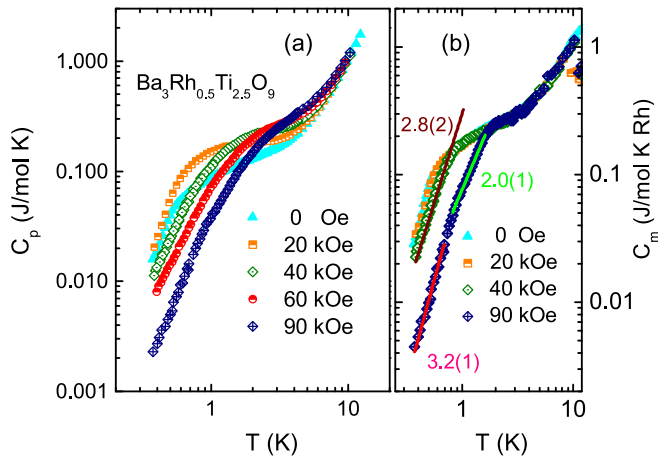

FIG. 8. (a) The heat capacity data for nominal Ba$_3$Rh$_{0.5}$Ti$_{2.5}$O$_9$ (AP/Baked) in log-log plot as a function of temperature at different fields. (b) The magnetic heat capacity C_m is shown in a log-log plot and the solid lines are fits to the power law: $C_m = \gamma T^\alpha$. The obtained exponent values are written against the C_m data.
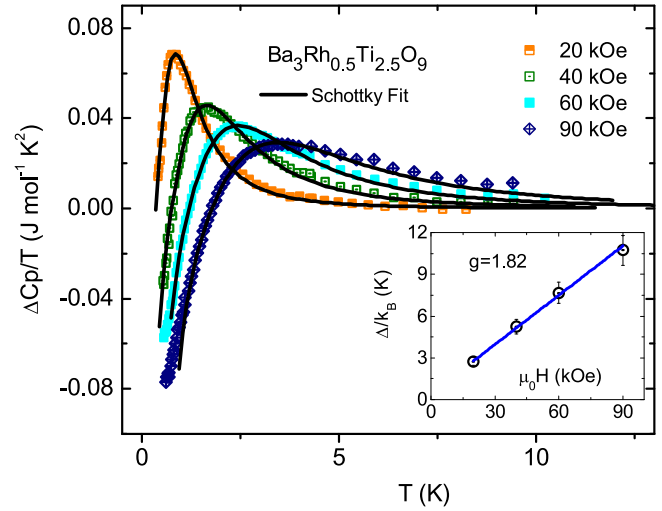

FIG. 9. A few representative plots of $[C_P(H) - C_P(H = 0)]/T$ or $(\triangle C_P/T)$ for nominal Ba$_3$Rh$_{0.5}$Ti$_{2.5}$O$_9$ at various values of the field H (as given in the legend) and their fit to Eq. (1) (black lines). (Inset) Variation of the Schottky gap as a function of magnetic field for orphan spins.

phase. This strongly diluted system seems to show no sign of LRO down to 0.35 K.

2. Magnetic susceptibility

The $\chi(T)$ of both the as-prepared batch (AP) of nominal Ba$_3$Rh$_{0.5}$Ti$_{2.5}$O$_9$ and few months older batch (ML), exposed to air, of nominal Ba$_3$Rh$_{0.5}$Ti$_{2.5}$O$_9$ did not show any difference in the ZFC-FC data [see the insets (a) and (b) of Fig. 7], respectively. The possibility of sample evolution/degradation with time/exposure to atmosphere was examined as this is known to happen in the high-T_c cuprates, the Na$_x$CoO$_2$ system [28], as also in the iridate material Na$_4$Ir$_3$O$_8$ [29]. Susceptibility data analysis for Ba$_3$Rh$_{0.5}$Ti$_{2.5}$O$_9$ as prepared (AP) batch gives $\chi_0 = -3.295 \times 10^{-4}$ cm^3/mole Rh, $\mu_{\text{eff}} \sim 1.78 \pm 0.18\,\mu_B$, and $\theta_{\text{CW}} \sim -154$ K. The $\chi(T)$ data for
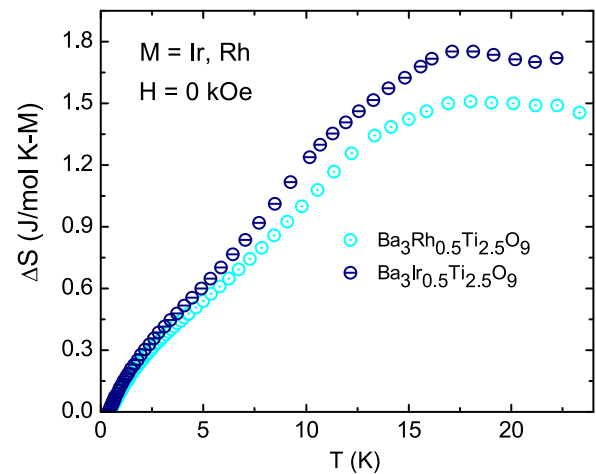

FIG. 10. Entropy change as a function of temperature for Ir and Rh variants at zero magnetic field for the nominal compositions of Ba$_3$Ir$_{0.5}$Ti$_{2.5}$O$_9$ and Ba$_3$Rh$_{0.5}$Ti$_{2.5}$O$_9$.
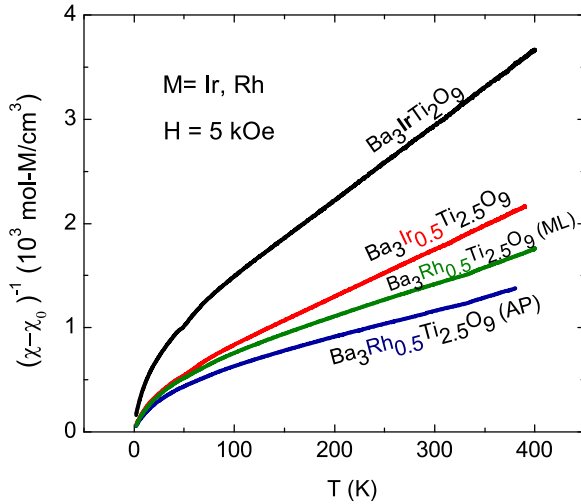
FIG. 11. Inverse susceptibility plots for Ir, Rh, and their variant samples (nominal composition) as a function of temperature. The data for $Ba_3IrTi_2O_9$ are taken from Ref. [4].

$Ba_3Rh_{0.5}Ti_{2.5}O_9$ and $Ba_3Ir_{0.5}Ti_{2.5}O_9$ suggest the formation of a quantum spin-liquid-like ground state in them. Also, neutron diffraction measurements done at 2 K, well below θ_{CW}, do not show any signatures of magnetic order for both the Rh-based compounds, and are in line with the susceptibility measurements. A comparison of susceptibility, μ_{eff} and θ_{CW} of the various Ir-based and Rh-based samples of this study are summarized in Fig. 11 and Table III, respectively.

3. Heat capacity

Now we present the $C_p(T)$ data obtained for nominal $Ba_3Rh_{0.5}Ti_{2.5}O_9$, which is single phase. The sample was first subject to heating at 200 °C for 10 hours. After the sample cooled back to room temperature, $C_p(T)$ measurements were performed soon after. To emphasize the low temperature $C_p(T)$ data of nominal $Ba_3Rh_{0.5}Ti_{2.5}O_9$, the data are only shown in the T-range 0.35–10 K, as can be seen in Fig. 8(a). The data are qualitatively similar to those for $Ba_3Ir_{0.5}Ti_{2.5}O_9$. In order to extract the magnetic heat capacity C_m, a similar process as mentioned before for nominal $Ba_3Ir_{0.5}Ti_{2.5}O_9$ was adopted. The estimation of Schottky contribution for nominal $Ba_3Rh_{0.5}Ti_{2.5}O_9$ from experimental data is shown in Fig. 9. The extracted orphan spin contribution (f) for $Ba_3Rh_{0.5}Ti_{2.5}O_9$ (nominal) amounts to 3%–4% of $S = 1/2$ entities. The g-factor estimated from plotting the Schottky gap data as a function of field for nominal $Ba_3Rh_{0.5}Ti_{2.5}O_9$ (see inset of Fig. 9) yields ~1.82. A value close to 2 suggests that the orphan spins do not suffer the effect of spin-orbit coupling.

The resulting C_m data for nominal $Ba_3Rh_{0.5}Ti_{2.5}O_9$ as a function of T and at various H are shown in Fig. 8(b). Here again the C_m for nominal $Ba_3Rh_{0.5}Ti_{2.5}O_9$ exhibits a variation similar to that of nominal $Ba_3Ir_{0.5}Ti_{2.5}O_9$ and can be fit with a power law in the low-T range. The exponent in the power-law at low temperature is somewhat H-dependent. Furthermore, the estimated entropy change for nominal $Ba_3Rh_{0.5}Ti_{2.5}O_9$ (see Fig. 10) does not recover the full value 5.76 J/mol K expected for ordered spin-1/2 moments. This downshift in entropy is a common tendency of frustrated spin systems. Similarly, below 20 K, the estimated entropy change for $Ba_3Rh_{0.5}Ti_{2.5}O_9$ comes out to be 1.78 J/mol K Rh. A comparison of entropy change for the studied compounds is tabulated in Table III.

IV. DISCUSSION

There has been a significant amount of work on a triangular variety of antiferromagnetic systems in the last few years. One issue that has been persistent among these systems, such as $Ba_3CuSb_2O_9$ (triangle or honeycomb) [13,18], Herbertsmithite (Kagome) [30–32], $SrCr_{9x}Ga_{12-9x}O_{19}$ (Kagome) [33,34], $Ba_3IrTi_2O_9$ (triangular biplanes) [4], or $Sc_2Ga_2CuO_7$ [35,36] (triangular biplanes), is the effect of vacancies at the magnetic sites. In minute amounts, these might simply give rise to an additional Curie term in the susceptibility and a Schottky like contribution to the heat capacity, keeping the correlated ground state intact. Experimental studies on the effect of percolation in magnetic systems are often limited to concentrations of dopants (nonmagnetic ions) where the LRO persists. In this region, the ordering temperature first falls linearly with an increase in the dopant concentration. Below the percolation threshold, magnetic LRO is destroyed. What might happen for even larger defect concentrations? It appears that there has been no experimental report on the work on (frustrated) triangular systems near the percolation threshold. A study on the layered honeycomb system $Mn_xZn_{1-x}PS_3$ [37] finds that below the percolation threshold, the high-temperature susceptibility data can be modeled as a combination of a term due to a randomly diluted antiferromagnet and a Curie term from uncompensated spins. The effective Curie-Weiss temperature and the Curie constant from the first term were found to *decrease* with increasing dopant concentration. In frustrated systems such as ours, one might expect to have a frozen/spin-glass state for a small concentration of nonmagnetic ions (i.e., above the percolation threshold) in case ordering is prevented. On going below the percolation threshold, a scenario as in $Mn_xZn_{1-x}PS_3$ might present itself in case of random occupation of Ir and Ti (in our system). For a bilayer triangular system (our case), the percolation

TABLE III. Estimated values of the Curie-Weiss temperature, the effective magnetic moment, the entropy change, and the magnetic heat capacity exponent for various compounds studied in this paper.

Compound	$\theta_{CW}(K)$	$\mu_{eff}(\mu_B)$	ΔS (J mol^{-1} K^{-1})	$C_m(T)$ exponent α	Reference
$Ba_3IrTi_2O_9$	−107	1.05 ± 0.04	0.57	1.9	[4]
$Ba_3Ir_{0.5}Ti_2O_9$	−125	1.32 ± 0.05	1.76	2.5	This work
$Ba_3Rh_{0.5}Ti_{2.5}O_9$ (AP)	−162	1.78 ± 0.18	1.51	3.2	This work
$Ba_3Rh_{0.5}Ti_{2.5}O_9$ (ML)	−149	1.58 ± 0.16	not measured		This work

threshold might be somewhat lower than that of a triangular lattice (site percolation p$_c$ = 0.5). In any case, for the two Ir (or Ti) concentrations studied by us (magnetic ion fraction 1/2 and 1/4) the Curie-Weiss temperature and the Curie constant *increase* slightly with increasing Ti concentration. For the Ba$_3$Rh$_{0.5}$Ti$_{2.5}$O$_9$ composition, a similar Curie-Weiss temperature was obtained. In case of a statistical occupancy, the probability of finding r Ir neighbours in the plane for an Ir (or Rh) within a plane is $^6C_r(p)^r(1-p)^{6-r}$, where p is the fraction of Ir (or Rh). Clearly, the probabilities of finding various clusters change significantly when p changes from 1/2 to 1/4. However, neither our Curie constants (or Curie-Weiss temperatures) nor the fraction contributing to the Schottky anomaly in the heat capacity change significantly. This suggests that Ti and Ir (or Rh) occupancy in the biplanes might not be at random. In fact, in Ba$_3$RuTi$_2$O$_9$, electronic structure calculations [38] have suggested that Ru-Ti dimers are energetically more stable than Ru-Ru or Ti-Ti dimers. A similar argument may be applicable for Ba$_3$IrTi$_2$O$_9$ (as also Ba$_3$Ir$_{0.5}$Ti$_{2.5}$O$_9$ and Ba$_3$Rh$_{0.5}$Ti$_{2.5}$O$_9$) and there might be some site ordering within the biplanes which could lead to continued connectivity in spite of the apparent depletion. Further work such as determination of the pair distribution function via high statistics diffraction data would be useful to settle this matter. Another possibility arises from the recent effort to explore the role of disorder in stabilising a spin liquid state in systems such as the subject of these papers ([19,39]). These have suggested that orphan spins that result from vacancy/disorder might remain delocalized and hence actually help in preventing freezing and stabilize a spin liquid state. Another point to note is that the effective moments (estimated from the Curie terms) are much smaller than those expected from pure spin-only values. This is possibly due to a spin-orbit coupling since it is seen that in going from 5d-based (Ir) to 4d-based (Rh) to 3d-based systems (Cu, in SGCO [35]) the effective moment goes up with the full spin only value being attained for the 3d case. In all the above situations, the spin-liquid state seems to be preserved suggesting that it is the

lattice geometry which drives this rather than any spin-orbit coupling effect. Electron or hole doping might be interesting to tune the ground states of these systems.

V. CONCLUSIONS

In summary, we have introduced a new 4d based, Rh^{4+} ($S =$ 1/2), bitriangular lattice system Ba$_3$Rh$_{0.5}$Ti$_{2.5}$O$_9$ (nominal) and in addition, also have studied the effect of dilution on its 5d analog Ba$_3$Ir$_{0.5}$Ti$_{2.5}$O$_9$ (nominal) via x-ray, neutron diffraction, magnetization, and heat capacity measurements. Our xrd/neutron refinement results infer the presence of highly depleted magnetic biplanes. The dc susceptibility measurements do not show any signature of magnetic order, glassiness or spin-freezing behavior for the freshly prepared/baked samples. Further, the measured heat capacity down to 0.35 K, well below the exchange energy, is found to be free from any kind of magnetic order and suggests the persistence of a QSL ground state for all of the materials studied. The novelty of these 4d/5d based materials is that in spite of the large depletion, they maintain strong antiferromagnetic couplings and retain the QSL ground state. Further local probe measurements like NMR and μSR will be of great importance to shed deeper insight into the intrinsic susceptibility (in presence of disorder) and the homogeneity of the ground state, respectively.

[1] W. Witczak-Krempa, G. Chen, Y. B. Kim, and L. Balents, Annu. Rev. Condens. Matter Phys. **5**, 57 (2014).

[2] G. Khaliullin, Phys. Rev. Lett. **111**, 197201 (2013).

[3] L. Balents, Nature (London) **464**, 199 (2010).

[4] T. Dey, A. V. Mahajan, P. Khuntia, M. Baenitz, B. Koteswararao, and F. C. Chou, Phys. Rev. B **86**, 140405(R) (2012).

[5] T. Dey, A. V. Mahajan, R. Kumar, B. Koteswararao, F. C. Chou, A. A. Omrani, and H. M. Ronnow, Phys. Rev. B **88**, 134425 (2013).

[6] Y. Okamoto, M. Nohara, H. Aruga-Katori, and H. Takagi, Phys. Rev. Lett. **99**, 137207 (2007).

[7] M. A. de Vries, A. C. Mclaughlin, and J.-W. G. Bos, Phys. Rev. Lett. **104**, 177202 (2010).

[8] T. Aharen, J. E. Greedan, C. A. Bridges, A. A. Aczel, J. Rodriguez, G. MacDougall, G. M. Luke, T. Imai, V. K. Michaelis, S. Kroeker, H. Zhou, C. R. Wiebe, and L. M. D. Cranswick, Phys. Rev. B **81**, 224409 (2010).

[9] J. P. Carlo, J. P. Clancy, T. Aharen, Z. Yamani, J. P. C. Ruff, J. J. Wagman, G. J. Van Gastel, H. M. L. Noad, G. E. Granroth, J. E. Greedan, and H. A. Dabkowska, and B. D. Gaulin, Phys. Rev. B **84**, 100404(R) (2011).

[10] M. A. de Vries, J. O. Piatek, M. Misek, J. S. Lord, H. M. Rnnow, and J. W. G. Bos, New J. Phys. **15**, 043024 (2013).

[11] T. Susuki, N. Kurita, T. Tanaka, H. Nojiri, A. Matsuo, K. Kindo, and H. Tanaka, Phys. Rev. Lett. **110**, 267201 (2013).

[12] J. G. Cheng, G. Li, L. Balicas, J. S. Zhou, J. B. Goodenough, C. Xu, and H. D. Zhou, Phys. Rev. Lett. **107**, 197204 (2011).

[13] H. D. Zhou, E. S. Choi, G. Li, L. Balicas, C. R. Wiebe, Y. Qiu, J. R. D. Copley, and J. S. Gardner, Phys. Rev. Lett. **106**, 147204 (2011).

[14] T. Dey and A. V. Mahajan, Eur. Phys. J. B **86**, 247 (2013).

[15] A. Nag, S. Middey, S. Bhowal, S. K. Panda, R. Mathieu, J. C. Orain, F. Bert, P. Mendels, P. G. Freeman, M. Mansson, H. M. Ronnow, M. Telling, P. K. Biswas, D. Sheptyakov,

S. D. Kaushik, V. Siruguri, C. Meneghini, D. D. Sarma, I. Dasgupta, and S. Ray, Phys. Rev. Lett. **116**, 097205 (2016).

[16] M. Becker, M. Hermanns, B. Bauer, M. Garst, and S. Trebst, Phys. Rev. B **91**, 155135 (2015).

[17] A. Catuneanu, J. G. Rau, H. S. Kim, and H. Y. Kee, Phys. Rev. B **92**, 165108 (2015).

[18] S. Nakatsuji, K. Kuga, K. Kimura, R. Satake, N. Katayama, E. Nishibori, H. Sawa, R. Ishii, M. Hagiwara, F. Bridges, T. U. Ito, W. Higemoto, Y. Karaki, M. Halim, A. A. Nugroho, J. A. Rodriguez-Rivera, M. A. Green, and C. Broholm, Science **336**, 559 (2012).

[19] A. Smerald and F. Mila, Phys. Rev. Lett. **115**, 147202 (2015).

[20] J. A. Quilliam, F. Bert, E. Kermarrec, C. Payen, C. Guillot-Deudon, P. Bonville, C. Baines, H. Luetkens, and P. Mendels, Phys. Rev. Lett. **109**, 117203 (2012).

[21] R. Skomski, *Simple Models of Magnetism* (Oxford University press, Oxford, 2008).

[22] P. Fischer, G. Frey, M. Koch, M. Könnecke, V. Pomjakushin, J. Schefer, R. Thut, N. Schlumpf, R. Bürge, U. Greuter, S. Bondt, and E. Berruyer, Physica B **276-278**, 146 (2000).

[23] R. J. Carvajal, Physica B **192**, 55 (1993).

[24] http://www.ncnr.nist.gov/resources/n-lengths/.

[25] M. A. de Vries, K. V. Kamenev, W. A. Kockelmann, J. Sanchez-Benitez, and A. Harrison, Phys. Rev. Lett. **100**, 157205 (2008).

[26] R. C. Byrne and C. W. Moeller, J. Solid State Chem. **2**, 228 (1970).

[27] K. E. Stitzer, M. D. Smith, J. Darriet, and H. C. zur Loye, Chem. Comm. **17**, 1680 (2001).

[28] K. Takada, H. Sakurai, E. Takayama-Muromachi, F. Izumi, R. A. Dilanian, and T. Sasaki, Nature (London) **422**, 53 (2003).

[29] R. S. Perry, K. Ohashi, K. Ihara, Y. Okamoto, T. Takayama, Fujiyama, N. Hussey, and H. Takagi (unpublished).

[30] J. S. Helton, K. Matan, M. P. Shores, E. A. Nytko, B. M. Bartlett, Y. Yoshida, Y. Takano, A. Suslov, Y. Qiu, J.-H. Chung, and D. G. Nocera, and Y. S. Lee, Phys. Rev. Lett. **98**, 107204 (2007).

[31] P. Mendels and F. Bert, J. Phys. Soc. Jpn. **79**, 011001 (2010).

[32] A. Olariu, P. Mendels, F. Bert, F. Duc, J. C. Trombe, M. A. de Vries, and A. Harrison, Phys. Rev. Lett. **100**, 087202 (2008).

[33] L. Limot, P. Mendels, G. Collin, C. Mondelli, B. Ouladdiaf, H. Mutka, N. Blanchard, and M. Mekata, Phys. Rev. B **65**, 144447 (2002).

[34] S. H. Lee, C. Broholm, G. Aeppli, T. G. Perring, B. Hessen, and A. Taylor, Phys. Rev. Lett. **76**, 4424 (1996).

[35] R. Kumar, P. Khuntia, D. Sheptyakov, P. G. Freeman, H. M. Rønnow, B. Koteswararao, M. Baenitz, M. Jeong, and A. V. Mahajan, Phys. Rev. B **92**, 180411(R) (2015).

[36] P. Khuntia, R. Kumar, A. V. Mahajan, M. Baenitz, and Y. Furukawa, Phys. Rev. B **93**, 140408(R) (2016).

[37] N. Chandrasekharan and S. Vasudevan, Phys. Rev. B **54**, 14903 (1996).

[38] G. Radtke, C. Maunders, A. Saúl, S. Lazar, H. J. Whitfield, J. Etheridge, and G. A. Botton, Phys. Rev. B **81**, 085112 (2010).

[39] T. Furukawa, K. Miyagawa, T. Itou, M. Ito, H. Taniguchi, M. Saito, S. Iguchi, T. Sasaki, and K. Kanoda, Phys. Rev. Lett. **115**, 077001 (2015).